ACS APPLIED MATERIALS & INTERFACES

Research Article

www.acsami.org

Bismuth Doped Lanthanum Ferrite Perovskites as Novel Cathodes for Intermediate-Temperature Solid Oxide Fuel Cells

Mei Li,[†] Yao Wang,[†,‡] Yunlong Wang,[†] Fanglin Chen,[‡] and Changrong Xia*[,†]

[†]CAS Key Laboratory of Materials for Energy Conversion, Department of Materials Science and Engineering& Collaborative Innovation Center of Suzhou Nano Science and Technology, University of Science and Technology of China, Hefei, Anhui 230026, China

[‡]Department of Mechanical Engineering, University of South Carolina, Columbia, South Carolina 29208, United States

Supporting Information

ABSTRACT: Bismuth is doped to lanthanum strontium ferrite to produce ferrite-based perovskites with a composition of $La_{0.8-x}Bi_xSr_{0.2}FeO_{3-\delta}$ ($0 \le x \le 0.8$) as novel cathode material for intermediate-temperature solid oxide fuel cells. The perovskite properties including oxygen nonstoichiometry coefficient (δ), average valence of Fe, sinterability, thermal expansion coefficient, electrical conductivity (σ), oxygen chemical surface exchange coefficient (K_{chem}), and chemical diffusion coefficient (D_{chem}) are explored as a function of bismuth content. While σ decreases with x due to the reduced Fe^{4+} content, D_{chem} and K_{chem} increase since the oxygen vacancy concentration is increased by Bi doping. Consequently, the electrochemical performance is substantially improved and the interfacial polarization resistance is reduced from 1.0 to 0.10 Ω cm^2 at 700 °C with Bi doping. The perovskite with x = 0.4 is suggested as the most promising composition as solid oxide fuel cell cathode material since it has demonstrated high electrical conductivity and low interfacial polarization resistance.

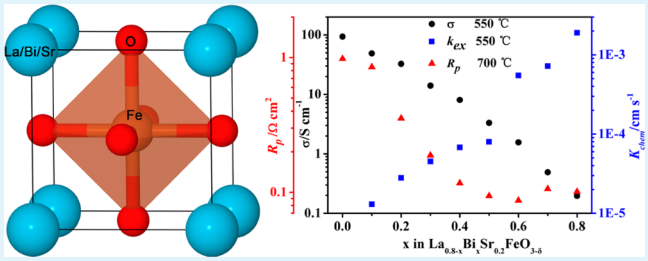

KEYWORDS: *solid oxide fuel cells, cathode, lanthanum strontium ferrite, bismuth doping, transport properties*

INTRODUCTION

Solid oxide fuel cells (SOFCs) can convert chemical energy in the fuel directly to electrical energy with fuel flexibility, high efficiency and low emissions.[1] In SOFCs, the cathode plays critical role since cathode polarization usually dominates in the total cell resistance. Consequently, there have been substantial interests in exploring novel cathode materials to reduce the cell polarization resistance in addition to reduce the operation temperature down to intermediate range (600−750 °C). As potential cathode materials for intermediate temperature SOFCs, ferrite-based perovskites have been studied to replace the conventional manganite based materials, typically strontium-doped lanthanum manganite (LSM).[2−4] Among various ferrite-based perovskites, strontium-doped lanthanum ferrite (LSF) has been extensively investigated since it exhibits high electrical conductivity.[5−9] For example, $La_{0.8}Sr_{0.2}FeO_{3-\delta}$ has a conductivity higher than 100 S cm^{-1} above 400 °C,[5,9,10] although some lower values (50−80 S cm^{-1}) have been reported in a larger temperature range.[6−8] Comparing with LSM, LSF has exhibited much higher electrochemical performance, i.e., much lower interfacial polarization resistance, R_p.[11] However, the cathode polarization resistance of LSF is still relatively high, e.g., R_p is 3.45 Ω cm^2 at 700 °C for $La_{0.8}Sr_{0.2}FeO_{3-\delta}$.[12] When the A-site lanthanum is replaced by bismuth, strontium-doped bismuth ferrite (BSF) has shown much higher electrochemical performance, and R_p is reduced to only 0.14 Ω cm^2 at 700 °C for $Bi_{0.7}Sr_{0.3}FeO_{3-\delta}$.[2] However, the electrical conductivity of BSF is relatively low, which can potentially limit its application when SOFCs are operated at high current densities. The maximum conductivity is below 1 S cm^{-1} for $Bi_{0.8}Sr_{0.2}FeO_{3-\delta}$ from 300 to 750 °C,[13] and it is only about 1 S cm^{-1} for $Bi_{0.7}Sr_{0.3}FeO_{3-\delta}$ between 300 and 900 °C.[2] Consequently, the high R_p values of LSF and the low electrical conductivity of BSF are the major barriers for application of ferrite-based materials as the SOFC cathodes. Although La^{3+} (1.22 Å) and Bi^{3+} (1.24 Å) have the same valence state and similar ionic radius, there are substantial differences in electrochemical performance and electrical conductivity due to the existence of highly polarizable $6s^2$ lone pair electrons for Bi^{3+} in comparison to La^{3+}.[14−16] Consequently, it will be valuable to explore the synergistic effect of La and Bi for ferrite-based perovskite, but there has been no systematic studies available.

In this work, bismuth is doped to the A-site of $La_{0.8}Sr_{0.2}O_{3-\delta}$ to form a series of ferrite-based perovskites with a general formula of $La_{0.8-x}Bi_xSr_{0.2}FeO_{3-\delta}$, where x = 0.0−0.8. These compounds are prepared using a combustion process and their lattice parameters, electrical conductivities, sintering behaviors, and oxygen transport properties are systematically evaluated as a function of the Bi content. The effects of Bi contents on the

Received: March 22, 2014
Accepted: June 27, 2014
Published: June 27, 2014

   dx.doi.org/10.1021/am5017045 | ACS Appl. Mater. Interfaces 2014, 6, 11286−11294

electrochemical performances are also evaluated using samaria doped ceria (SDC) as the electrolyte.

EXPERIMENTAL SECTION

Materials Synthesis. $La_{0.8-x}Bi_xSr_{0.2}FeO_{3-\delta}$ (LBSF, x = 0–0.8) powders were synthesized using a combustion process with ethylenediaminetetraacetic acid (EDTA) and citric acid as the combustion agents. The cation precursors were $Bi(NO_3)_3{\cdot}5H_2O$ (99.0%), $Sr(NO_3)_2$ (99.5%), $Fe(NO_3)_3{\cdot}9H_2O$ (98.5%), and La_2O_3 (99.99%). La_2O_3 was dissolved in nitric acid to form lanthanum nitrate. Aqueous nitrate solutions were formed by adding stoichiometric amounts of the nitrate precursors to distilled water. The combustion agents were subsequently added to the nitrate solution with a molar ratio of 1:1:2 for the total metal ions, EDTA (99.5%), and citric acid (99.5%), respectively. The pH was adjusted to about 6.0 with ammonia. The mixed solution was then stirred for 2 h with magnetic stirring apparatus before it was heated on a hot plate until self-combustion occurred. The as-prepared ash was collected and heated at 800 °C for 2 h to form the required powders. $Sm_{0.2}Ce_{0.8}O_{1.9}$ (SDC) was prepared using the carbonate coprecipitation method.[17] $Sm(NO_3)_3$ (99.95%) and $Ce(NO_3)_3$ (99%) were used as the cation sources, and ammonia carbonate (99.7%) was used as the precipitant. The precipitates were dried at 90 °C and then calcined at 600 °C for 2 h to obtain SDC powders with fluorite structure. All chemicals were from Sinopharm Chemical Reagent Co. Ltd.

Transport Properties. LBSF bars were prepared to determine the transport properties, including electrical conductivity, chemical surface exchange coefficient (K_{chem}) and chemical diffusion coefficient (D_{chem}). The measurement was conducted using a four-probe method with a digital multimeter (Keithley, 2001-785D). The bar samples with dimension of 1.0 × 5.5 × 16 mm^3 were fabricated with the LBSF powders, which were uniaxially pressed at 300 MPa, followed by sintering at temperatures ranged from 900 to 1225 °C for 5 h in air to ensure high relative density, over 95% of the theoretical density as determined with the Archimedes drainage method. The K_{chem} and D_{chem} values were determined using electrical conductivity relaxation (ECR) method.[18−20] To conduct the ECR measurement, LBSF bars were placed in a quartz tube, heated to a high temperature and then stabilized for about 1 h to make sure they were completely equilibrated with the surrounding atmosphere of air (P_{O_2} = 0.21 atm), and the atmosphere was then rapidly changed to pure oxygen (P_{O_2} = 1 atm). The increase in P_{O_2} led to electrical conductivity change, which was recorded, normalized and fitted to a solution of Fick's second law to obtain D_{chem} and K_{chem}.[21] Gas flow was fixed at 200 mL min^{-1} to ensure that the time spent to achieve gas concentration equilibrium was no more than 20 s. Electrical conductivities were recorded using a dc four-probe technique, where four silver wires were attached to the sample as the lead wires, and silver paste (Sina-Platinm Metals Co., Ltd.) was used to improve the contacts between the wires and the sample. The experimental temperature was in the range from 550 to 800 °C.

Electrochemical Properties of LBSF Electrodes. Symmetrical cells with the configuration of LBSF/SDC/LBSF were prepared for electrochemical characterization. The SDC powders were uniaxially pressed at 250 MPa and then sintered at 1400 °C for 5 h to form dense SDC pellets as the electrolyte substrates, which were about 10 mm in diameter and 0.5 mm thick. LBSF powders were mechanically mixed with organic additives (α-terpineol and ethyl cellulose) to form a slurry with 40 wt % LBSF. The slurry was then printed to both sides of the SDC pellets using the screen-printing technique, and subsequently calcined at 850 °C for 2 h in air to form porous LBSF electrodes. The interfacial polarization resistance of the symmetrical cells was determined from ac impedance spectroscopy using Solartron 1260 impedance/gain-phase analyzer in ambient air with the frequency in the range of 0.01 Hz to 1 MHz and a bias voltage of 10 mV.

The electrochemical performance of $La_{0.4}Bi_{0.4}Sr_{0.2}FeO_{3-\delta}$ cathode is further characterized using single cells with Ni-SDC anode substrates and SDC film electrolytes. The anode powders consisting of 60 wt % NiO and SDC were mixed and pressed at 30 MPa. SDC powder as the electrolyte was subsequently added on the top of the prepressed anode pellet and then copressed at 180 MPa to form a green bilayer structure: a thin SDC layer supported on a thick NiO-SDC layer.[22] The bilayers were sintered at 1375 °C for 5 h to densify the electrolyte. $La_{0.4}Bi_{0.4}Sr_{0.2}FeO_{3-\delta}$ slurry was then applied on the surface of the dense electrolyte and fired at 850 °C for 2 h.

Characterizations. The phase structures were investigated using X-ray diffraction (XRD, Rigaku TTR-III diffractmeter) with Cu Kα radiation source. The XRD patterns were obtained in the range of 20–80° with a 0.02° step size and a scan speed of 1°/min at 40 kV and 200 mA, and the initial intensity of peaks for all the spectra were about 20000 CPS. Oxygen nonstoichiometry coefficient, average Fe valence and crystalline parameters were calculated from the XRD data using the Rietveld refinement method. To evaluate the chemical compatibility between LBSF electrode and SDC electrolyte at fuel cell operation and electrode fabrication temperatures, $La_{0.8-x}Bi_xSr_{0.2}FeO_{3-\delta}$ (x = 0.0, 0.4, 0.8) powders were mixed with SDC powders with weight ratio of 1:1. The mixture was heated at 850 °C for 5 h, forming LBSF-SDC composites for XRD measurement. The thermal expansion behavior and sintering process were investigated using a dilatometer (NETZSCH DIL402C, Germany) at a heating rate of 5 °C/min. The microstructures were characterized using scanning electron microscopy (SEM, JSM-6700F).

RESULTS AND DISCUSSION

Phase Structures. Figure 1a shows the X-ray diffraction patterns for the LBSF powders, which have been heated at 800 °C for 2 h. The XRD pattern exhibits well-crystallized perovskite structure without any observable secondary phases. The samples show cubic structure when $x \geq 0.3$, while those show orthorhombic structure when $x \leq 0.2$. Figure 1b shows the magnified view of the XRD patterns for (020) lattice plane.

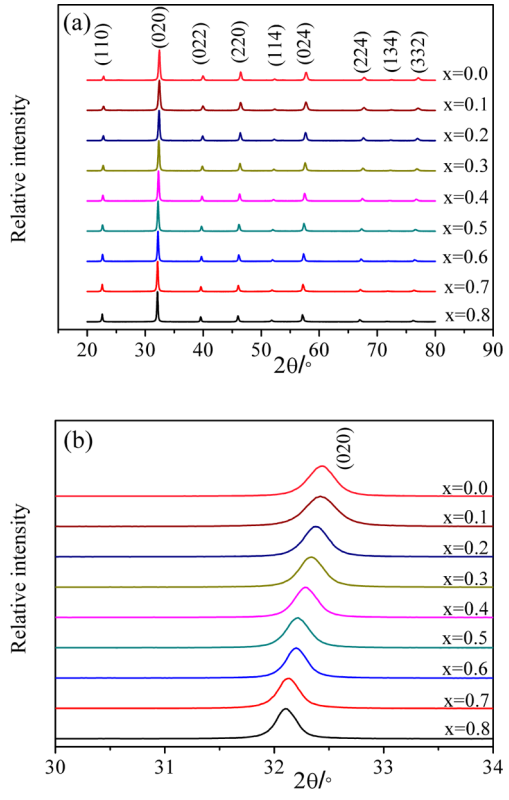

Figure 1. (a) X-ray diffraction patterns of $La_{0.8-x}Bi_xSr_{0.2}FeO_{3-\delta}$ powders with various Bi contents and (b) the magnified view for the (020) peak.

dx.doi.org/10.1021/am5017045 | ACS Appl. Mater. Interfaces 2014, 6, 11286–11294

With an increase in the bismuth content, the corresponding XRD peaks shift toward smaller angles, indicating expansion of the lattice volume within the same crystal structure, possibly caused by the relatively larger Bi^{3+} (1.24 Å) than La^{3+} (1.22 Å) in addition to oxygen vacancy formation, which will be discussed later. Oxygen nonstoichiometry coefficient (δ), average Fe valence (n), as well as lattice parameters (a, b, and c) are calculated from the XRD patterns by Rietveld refinement[23] and listed in Table 1. The values of R_p and R_{wp}

Table 1. Lattice Parameters (a, b, and c), Oxygen Nonstoichiometry Coefficient (δ) and Average Fe Valence (n) of $La_{0.8-x}Bi_xSr_{0.2}FeO_{3-\delta}$

x	a (Å)	b (Å)	c (Å)	R_{wp} (%)	R_p (%)	δ	n
0.8	3.9533	3.9533	3.9533	7.25	5.44	0.100	3.002
0.7	3.9457	3.9457	3.9457	6.81	4.98	0.090	3.020
0.6	3.9415	3.9415	3.9415	6.82	5.00	0.074	3.052
0.5	3.9353	3.9353	3.9353	6.54	4.75	0.042	3.116
0.4	3.9292	3.9292	3.9292	6.38	4.44	0.030	3.140
0.3	3.9256	3.9256	3.9256	6.72	4.55	0.021	3.158
0.2	5.5476	5.5405	7.8317	6.47	4.51	0.012	3.176
0.1	5.5462	5.5330	7.8261	6.08	4.04	0.006	3.188
0.0	5.5490	5.5261	7.8190	7.83	4.90	0.001	3.200

indicate the good quality of the simulation. The good agreement between the calculated and experimental XRD profiles of $La_{0.4}Bi_{0.4}Sr_{0.2}FeO_{3-\delta}$ is presented as an example, Figure 2. When the Bi content (x) increases, δ increases, n

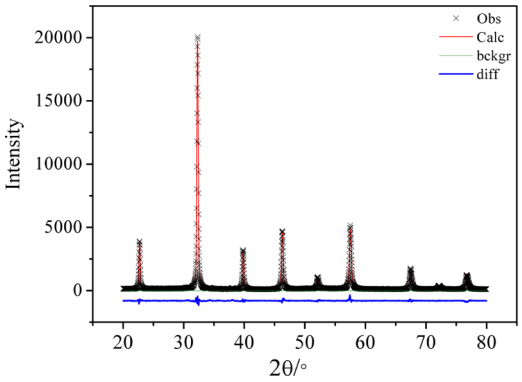

Figure 2. Rietveld refinement plot of $La_{0.4}Bi_{0.4}Sr_{0.2}FeO_{3-\delta}$.

decreases, while the lattice parameter for the cubic phase increases. The highest δ is 0.1 for $Bi_{0.8}Sr_{0.2}FeO_{2.9}$ and the greatest value of n is 3.2 for $La_{0.8}Sr_{0.2}FeO_{2.999}$.

In the $La_{0.8-x}Bi_xSr_{0.2}FeO_{3-\delta}$ perovskites, δ value represents oxygen vacancy content. Therefore, δ increases with x demonstrating that Bi doping can increase the oxygen vacancy content. Bi^{3+}cation has highly polarizable $6s^2$ lone pair electrons. Oxygen ions adjacent to the lone pair electron plane can leave the structure easily, that is, the relaxation of the structure should be easier in the proximity of these lone pair electrons than in any other places in the network.[24,25] When x increases, the concentration of the lone pair electrons increases, facilitating the defect formation, and consequently leading to an increase in the oxygen vacancy content. Meanwhile, the lattice volume increases due to the enhanced repulsion force between those mutually exposed cations when oxygen ions are extracted from the lattice in addition to the increase in cation size of Fe ions from higher to lower valence associated with the creation of oxygen vacancies.[26]

Figure 3 is the XRD patterns for SDC as well as the LBSF-SDC composites. The XRD pattern of the composite can be

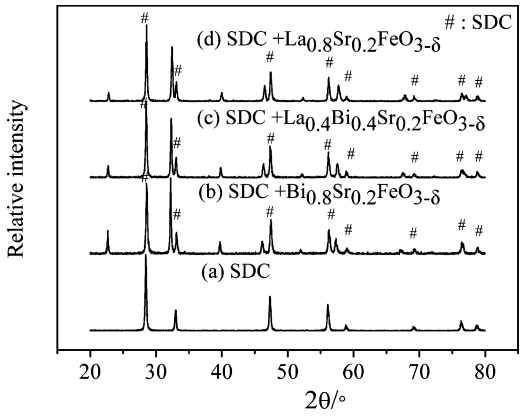

Figure 3. XRD patterns of (a) SDC powder fired at 600 °C for 2 h, and (b–d) the composites of SDC and $La_{0.8-x}Bi_xSr_{0.2}FeO_{3-\delta}$ (x = 0.8, 0.4, 0.0) fired at 850 °C for 5 h.

attributed to either LBSF or SDC, indicating that there is no detectable chemical reaction between SDC and LBSF under the experimental conditions. The results further demonstrate that LBSF is chemically compatible with SDC under the electrode fabrication and typical fuel cell operating conditions.

Sintering Characteristics. Figure 4a shows the shrinkage curves of the $La_{0.8-x}Bi_xSr_{0.2}FeO_{3-\delta}$ bars with different compositions where x = 0.0, 0.2, 0.4, 0.6, and 0.8. The bars were formed by pressing the corresponding powders at room temperature. It

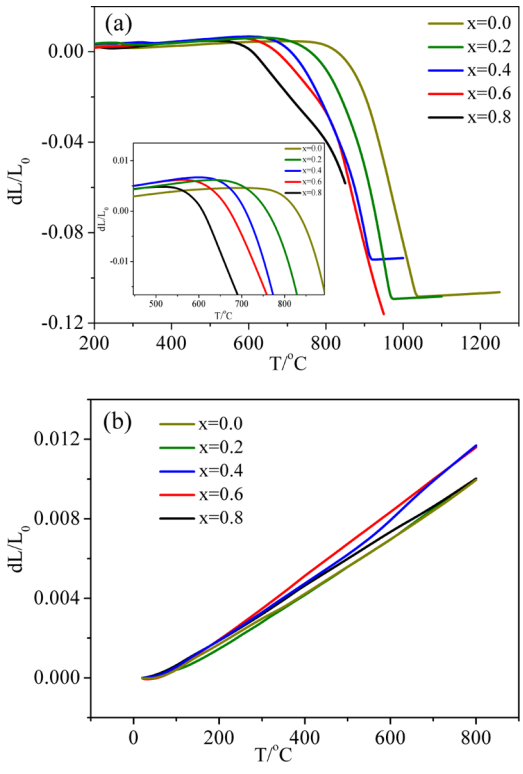

Figure 4. (a) Sintering curves and (b) thermal expansion curves for $La_{0.8-x}Bi_xSr_{0.2}FeO_{3-\delta}$ (x = 0.0, 0.2, 0.4, 0.6, 0.8).

dx.doi.org/10.1021/am5017045 | ACS Appl. Mater. Interfaces 2014, 6, 11286–11294

Table 2. Conductivity (σ, S cm^{-1}) at 700 °C, Activation Energy (E_a, eV) for Conductivity, Sintering Temperature (T, °C), Thermal Expansion Coefficient (TEC, 10^{-6} K^{-1}), and Relative Density (ρ_r, %) of $La_{0.8-x}Bi_xSr_{0.2}FeO_{3-\delta}$

x	0.0	0.1	0.2	0.3	0.4	0.5	0.6	0.7	0.8
E_a	0.073	0.120	0.132	0.136	0.140	0.182	0.258	0.395	0.563
σ	94.6	55.0	37.8	16.5	9.3	4.2	2.3	0.98	0.56
T	1225	1190	1160	1100	1065	1040	1000	980	900
ρ_r	98.2	98.6	97.4	98.0	97.8	97.7	97.9	98.3	95.1
TEC	13.1	13.8	13.7	14.0	14.8	14.6	15.9	14.5	13.6

can be seen that $La_{0.8}Sr_{0.2}FeO_{3-\delta}$ starts to sinter at about 780 °C. When La is partially replaced by Bi, the sintering temperature is reduced from 780 to 700 °C for x = 0.2, to 650 °C for x = 0.4, and to about 600 °C for x = 0.6. Finally, when La is completely replaced by Bi, the sintering temperature decreases to 550 °C for $Bi_{0.8}Sr_{0.2}FeO_{3-\delta}$. Consequently, Bi doping reduces the sintering temperature, which might be caused by the relatively low melting point of Bi_2O_3, which is only 860 °C. Therefore, the sintering temperature is different for $La_{0.8-x}Bi_xSr_{0.2}FeO_{3-\delta}$ with various doping level x. Table 2 lists the sintering temperature and relative density. Figure 4b shows the typical thermal expansion behaviors of $La_{0.8-x}Bi_xSr_{0.2}FeO_{3-\delta}$. The average thermal expansion coefficient (TEC) is calculated from the thermal expansion curves and the values are presented in Table 2. The TEC value for $La_{0.8}Sr_{0.2}FeO_{3-\delta}$ is 13.1 × 10^{-6} K^{-1}, close to 12.6 × 10^{-6} K^{-1} as reported by Tai et al.[25] The effect of Bi doping on TEC is much complicated. Usually, TEC increases with oxygen vacancy concentration.[27] In the low temperature range, the concentration increases with x. When the temperature increases, some Fe^{4+} change to Fe^{3+}, generating more oxygen vacancies.[28] Since the average Fe valence (n) decreases with x, less vacancies are yielded at high temperature for $La_{0.8-x}Bi_xSr_{0.2}FeO_{3-\delta}$ with larger x. Figure 5 shows the surface morphology of $La_{0.8-x}Bi_xSr_{0.2}FeO_{3-\delta}$ (x =0.0, 0.4, 0.8) bars. Although the sintering temperature of $La_{0.4}Bi_{0.4}Sr_{0.2}FeO_{3-\delta}$ is higher than that of $Bi_{0.8}Sr_{0.2}FeO_{3-\delta}$, they have a similar average grain size of about 0.2 μm. The grain size of $La_{0.8}Sr_{0.2}FeO_{3-\delta}$ is about 1.0 μm.

Electrical Conductivities. Figure 6 shows LBSF electrical conductivity measured in air. At the same temperature, the conductivity decreases upon increasing x, Figure 6a. The highest conductivity is observed for the sample without bismuth, $La_{0.8}Sr_{0.2}FeO_{3-\delta}$. At 700 °C, it is 94.6 S cm^{-1}, in good agreement to 93 S cm^{-1} at the same temperature reported by Tai et al.[26] It is noted that the electrical conductivities of $La_{0.8}Sr_{0.2}FeO_{3-\delta}$ at temperatures above 400 °C are in the range from 50 to 125 S cm^{-1}.[5−10] The lowest conductivity is presented by $Bi_{0.8}Sr_{0.2}FeO_{3-\delta}$. At 700 °C, it is only 0.56 S cm^{-1}, similar to 0.49 S cm^{-1} reported by Anja et al. at the same temperature.[13] For the same sample, an increase in temperature leads to a steady increase in conductivity except for x = 0.7 and 0.8. The perovskites for $x \leq 0.4$ exhibit metallic and semiconducting behavior, while the others show semiconducting behavior. The relationships between $1/T$ and $\ln(\sigma T)$ in Arrhenius plots are shown in Figure 6b, indicating that the thermally activated hopping of small polarons dominates in these materials when $T \leq 700$ °C.[29,30] The activation energy (E_a) for conductivity is determined from the linear part of the Arrhenius plot. The conductivities at 700 °C and activation energies are also listed in Table 2. The E_a value for $La_{0.8}Sr_{0.2}FeO_{3-\delta}$ is 0.073 eV while it is 0.563 eV for $Bi_{0.8}Sr_{0.2}FeO_{3-\delta}$. Obviously, E_a increases by bismuth doping.

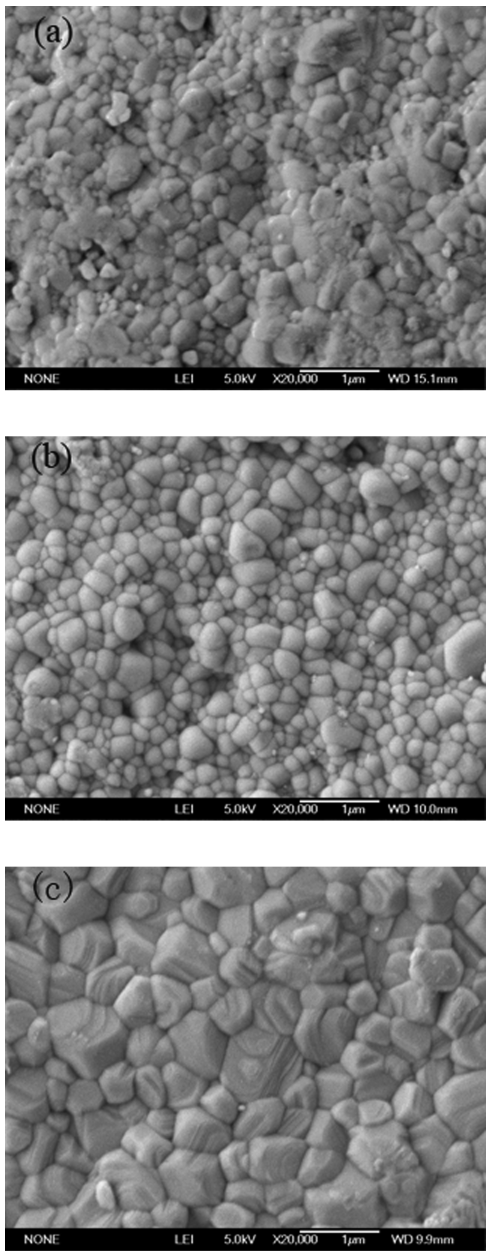

Figure 5. SEM graphs for the surface microstructures of $La_{0.8-x}Bi_xSr_{0.2}FeO_{3-\delta}$ bars (a) x = 0.8; (b) x = 0.4; (c) x = 0.0.

The total electrical conductivity from the sample is the sum of electronic and oxygen ionic conductivities. The electric conductivity is determined by the double exchange between oxygen ions and ferric ions, and the mechanistic model can be written as[31]

$$Fe^{3+} - O^{2-} - Fe^{4+} - O^{2-} - Fe^{3+}$$

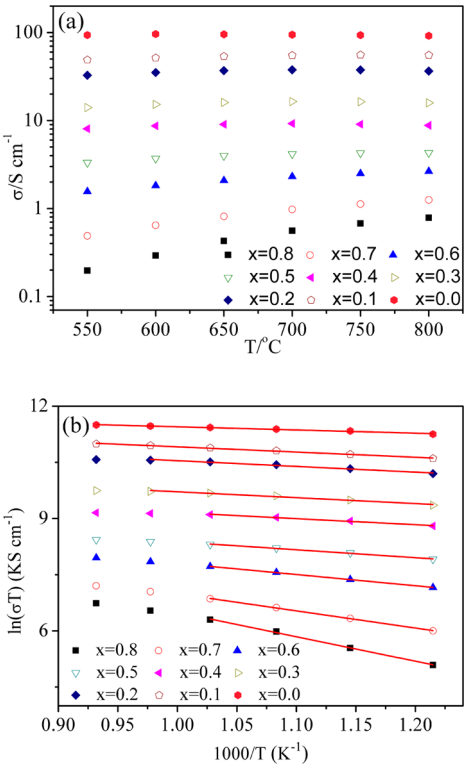

Figure 6. Conductivity (σ) for $La_{0.8-x}Bi_xSr_{0.2}FeO_{3-\delta}$. (a) σ versus temperature at various Bi content (x); (b) σT in Arrhenius form.

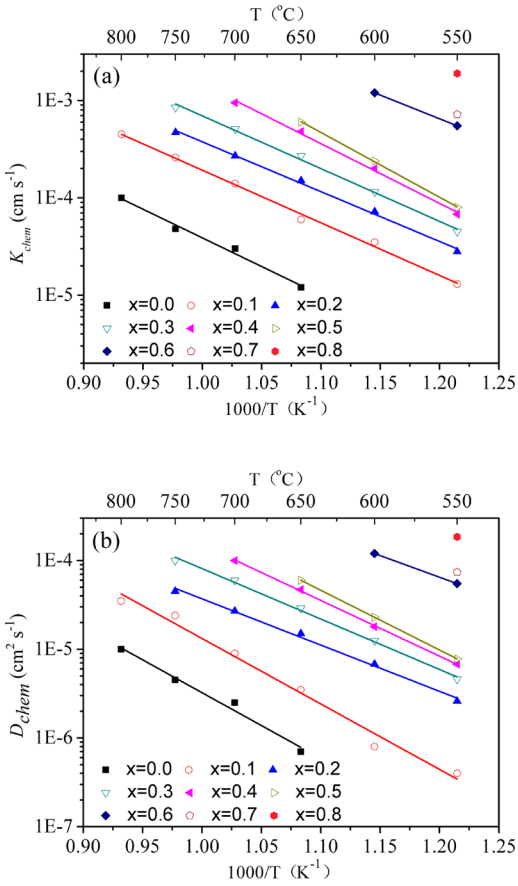

Figure 7. (a) Chemical surface exchange coefficient (K_{chem}) and (b) Chemical diffusion coefficient (D_{chem}) versus temperature for $La_{0.8-x}Bi_xSr_{0.2}FeO_{3-\delta}$.

The transport of the electrons along Fe^{3+}, O^{2-}, and Fe^{4+} contributes to the electronic conductivity. Since the content of Fe^{3+} is much higher than Fe^{4+}, the Fe^{4+} content determines the electronic conductivity. Table 1 shows that the average Fe valence state in these samples is higher than 3.0 and decreases with x. Therefore, increasing Bi content reduces the Fe^{4+} content, consequently reducing the electronic conductivity. The activation energy increases with x, implying increased oxygen ionic transfer number at higher Bi content. Since the oxygen vacancy concentration increases with x, the ionic conductivity should also increase with the Bi content.

Oxygen Transport Properties. The oxygen transport properties are determined using the ECR method. The transport kinetics are obtained by fitting the experimental data (Figure S1(a–h)) and the K_{chem} and D_{chem} values are presented in Figure 7a,b, respectively. K_{chem} for $La_{0.8}Sr_{0.2}FeO_{3-\delta}$ obtained in this study is consistent with that reported in the literature. For example, at 650 °C, K_{chem} is 1.2×10^{-5} cm s^{-1}, close to 1.0×10^{-5} cm s^{-1} and at 700 °C, K_{chem} is 3.0×10^{-5} cm s^{-1}, equal to that reported by la O' et al.[32] At 800 °C, the relaxation time is about 2.5×10^3 s for $La_{0.8}Sr_{0.2}FeO_{3-\delta}$ and increases upon decreasing temperature. At 650 °C, it increases to 1.6×10^4 s, and further to 2.2×10^4 s at 600 °C. The much longer equilibrium time makes it difficult to fit the experimental results well. Therefore, the transport properties for $La_{0.8}Sr_{0.2}FeO_{3-\delta}$ at 600 and 500 °C can not be obtained with the ECR method. D_{chem} (1.85×10^{-4} cm^2 s^{-1}) and K_{chem} (1.9×10^{-3} cm s^{-1}) for $Bi_{0.8}Sr_{0.2}FeO_{3-\delta}$ are only measured at 550 °C, and the relaxation time is about 150 s and decreases with increasing temperature, which reduces the reliability of the results.[33,34] Consequently, the transport properties at temperature higher than 550 °C are not measured for $Bi_{0.8}Sr_{0.2}FeO_{3-\delta}$. Figure 7 shows that the transport properties, both surface exchange and oxygen bulk transport coefficients, are substantially improved by Bi doping.

The surface reaction can be written as[35]

$$\frac{1}{2}O_2(g) + V_O^{\cdot\cdot} + 2e' = O_O^{\times}$$

The reaction rate depends on the oxygen partial pressure Po_2, and the concentrations of oxygen vacancies and electrons. When P_{O_2} is fixed, the rate is controlled by the concentrations of oxygen vacancies and electrons. Since $La_{0.8-x}Bi_xSr_{0.2}FeO_{3-\delta}$ are predominately electronic conductors, their electron concentration are much larger than that of the oxygen vacancies. Therefore, surface reaction rate is limited by the oxygen vacancy concentration, which corresponds to δ. Meanwhile, the diffusion rate usually scales with the oxygen vacancy concentration. As described earlier, δ increases with Bi content (x). Consequently, D_{chem} and K_{chem} increase with x. It should be noted that D_{chem} and K_{chem} are different from the self-diffusion coefficient (D_o) and surface exchange coefficient (K_{true}), respectively. Theoretically, they can be related to the thermodynamic factor.[35,36]

Electrochemical Properties. To examine the electrochemical properties of LBSF, impedance spectra are measured at temperatures from 450 to 800 °C using symmetrical cell configuration with LBSF electrodes on the SDC electrolyte substrates. Figure 8a,b shows the interfacial polarization resistance at various temperatures. R_p generally decreases with Bi content, Figure 8a. At 700 °C, R_p is about 1.0 Ω cm^2 for

dx.doi.org/10.1021/am5017045 | ACS Appl. Mater. Interfaces 2014, 6, 11286–11294

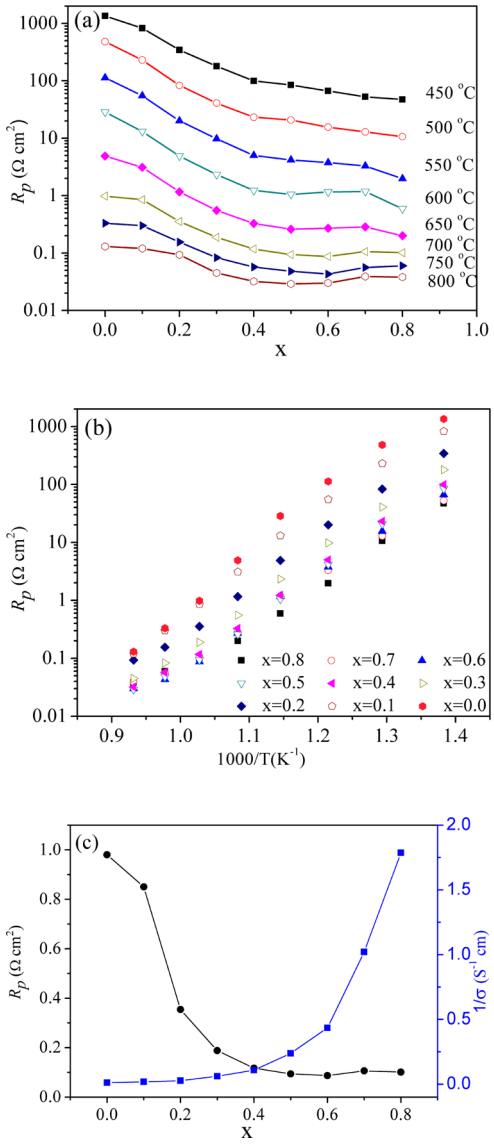

Figure 8. Interfacial polarization resistance (R_p) for $La_{0.8-x}Bi_xSr_{0.2}FeO_{3-\delta}$ electrode measured from 450 to 800 °C. (a) R_p versus Bi content (x); (b) R_p versus $1/T$; and (c) R_p and $1/\sigma$ versus x at 700 °C.

$La_{0.8}Sr_{0.2}FeO_{3-\delta}$. The performance is in good agreement with that (1.1 Ω cm^2 at 700 °C) reported for a $La_{0.7}Sr_{0.3}FeO_{3-\delta}$ electrode on a SDC electrolyte,[37] but is much smaller than 3.45 Ω cm^2 for $La_{0.8}Sr_{0.2}FeO_{3-\delta}$ electrode on a YSZ electrolyte reported by Martinez-Amesti et al.[12] The interfacial polarization resistance is reduced by adding bismuth and is 0.85 Ω cm^2 at 700 °C when x = 0.1. It further decreases to 0.10 Ω cm^2 at 700 °C when x = 0.8, i.e., $Bi_{0.8}Sr_{0.2}FeO_{3-\delta}$. It is noted that R_p is 0.12 Ω cm^2 at 700 °C when x = 0.4. Therefore, under open circuit conditions, $La_{0.4}Bi_{0.4}Sr_{0.2}FeO_{3-\delta}$ demonstrates similar electrochemical performance to $Bi_{0.8}Sr_{0.2}FeO_{3-\delta}$. Meanwhile, the electrical conductivity for $La_{0.4}Bi_{0.4}Sr_{0.2}FeO_{3-\delta}$ is more than 1 order of magnitude higher than $Bi_{0.8}Sr_{0.2}FeO_{3-\delta}$, Figure 8c. On the other hand, $La_{0.4}Bi_{0.4}Sr_{0.2}FeO_{3-\delta}$ demonstrates much better electrochemical performance than $La_{0.8}Sr_{0.2}FeO_{3-\delta}$. Figure 8c compares the interfacial polarization resistance and the electronic resistance of these materials. It clearly shows that x = 0.4 should be the best composition for $La_{0.8-x}Bi_xSr_{0.2}FeO_{3-\delta}$ perovskites as the cathode materials for intermediate-temperature SOFCs. It should be noted that the electrochemical performance could be further improved by adding electrolyte material to form a composite cathode such as LBSF-SDC.

The Nyquist plots and the fitting results with two arcs are presented in Figure 9a–c for the impedance spectra measured

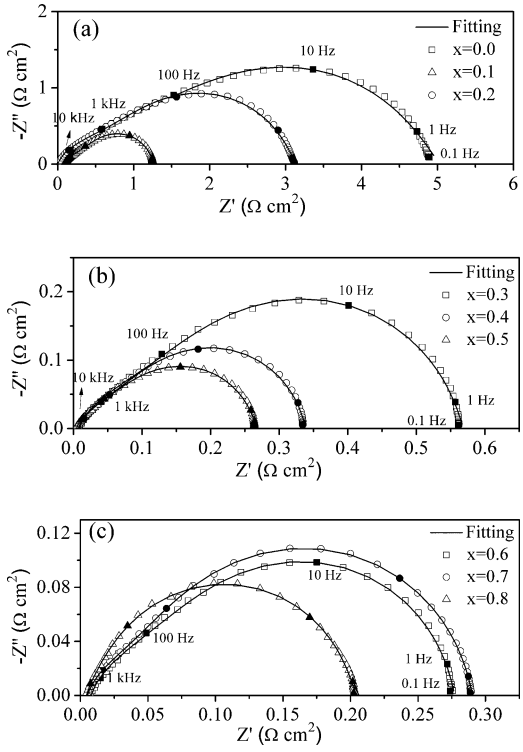

Figure 9. (a–c) Electrochemical impedance spectra (EIS) for $La_{0.8-x}Bi_xSr_{0.2}FeO_{3-\delta}$ symmetrical cells at 650 °C.

at 650 °C. Note that the ohmic resistance from the electrolyte and leading wires has been subtracted while the interfacial polarization resistance is divided by two in order to account for the contributions of two symmetrical electrodes. The impedance spectra could be separated to one high-frequency and one low-frequency arc. As suggested by Adler[38] and Escudero,[39] the high-frequency arc (R_H) corresponds to the charge transport step while the low-frequency arc (R_L) can be ascribed to the surface step. Figure 9 shows that both the high and low frequency arcs are reduced when Bi is doped. Furthermore, both R_H and R_L decrease with the increase of x, Figure 10, suggesting that Bi doping can accelerate the kinetics related to both oxygen ion transport and oxygen surface exchange, consistent with the ECR measurement, which has shown increased D_{chem} and K_{chem} values with x.

As shown in Figure 11, the activation energy (E_a) for R_p for different samples decreases with x: $La_{0.8}Sr_{0.2}FeO_{3-\delta}$ has the highest E_a (1.87 eV), consistent with the value of 1.9 eV reported by others,[40] while $Bi_{0.8}Sr_{0.2}FeO_{3-\delta}$ has the lowest E_a (1.40 eV). With the increase in Bi content, oxygen vacancy increases, and the energy barrier for oxygen adsorption and oxygen ion transport decreases correspondingly. Therefore, the catalytic activity increases with bismuth content, which in turn explains the decrease in R_p values with the increase in bismuth content for $La_{0.8-x}Bi_xSr_{0.2}FeO_{3-\delta}$.

The electrochemical performance of the $La_{0.4}Bi_{0.4}Sr_{0.2}FeO_{3-\delta}$ cathode is further characterized using a single cell with a Ni-SDC anode and a 30-μm-thick SDC electrolyte. Figure 12a

dx.doi.org/10.1021/am5017045 | ACS Appl. Mater. Interfaces 2014, 6, 11286–11294

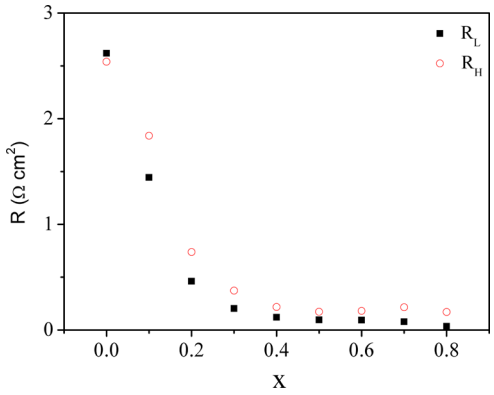

Figure 10. Resistance at 650 °C for the high-frequency (R_H) and low-frequency (R_L) arcs of $La_{0.8-x}Bi_xSr_{0.2}FeO_{3-\delta}$.

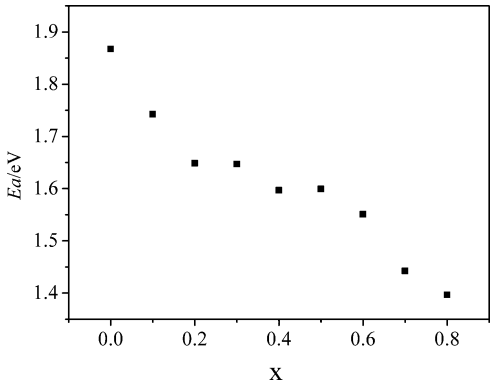

Figure 11. Activation energy (E_a) of R_p for $La_{0.8-x}Bi_xSr_{0.2}FeO_{3-\delta}$.

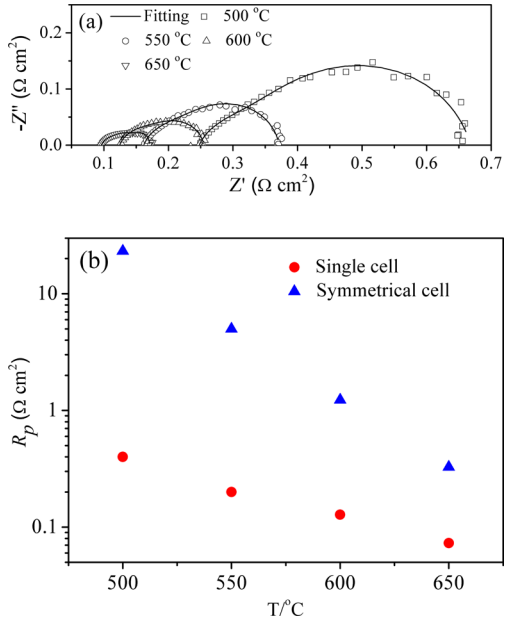

Figure 12. (a) Electrochemical impedance spectra (EIS) for a single cell with $La_{0.4}Bi_{0.4}Sr_{0.2}FeO_{3-\delta}$ cathode and (b) R_p obtained with the symmetrical cell and the single cell.

shows the impedance spectra for the single cell operated with humidified H_2 as the fuel and ambient air as the oxidant. The interfacial polarization resistance between the two intercepts at the real axis is contributed by both the cathode and the anode. For an anode supported single cell operated with H_2 fuel, the anode polarization resistance is usually negligible.[41] Therefore, the total cell polarization resistance is dominated by the cathode. Figure 12b compares the resistances obtained with the single cell and the symmetrical cell. It is obvious that the resistance from the single cell is much lower than the symmetrical cell. Since the electronic conduction in SDC is not negligible under the fuel cell conditions, the interfacial resistance derived from the single cell is much lower than the symmetrical cell, where the electronic conduction is negligible.[42] In addition, the small resistance could be attributed to the activation effect, which is common in perovskite cathode materials such as LSM and $La_{0.6}Sr_{0.4}Co_{0.2}Fe_{0.8}O_{3-\delta}$ (LSCF).[43] The single cell generates a peak power density of 480 mW cm^{-2} at 600 °C. The performance is comparable to those obtained with composite cathodes such as $Sm_{0.5}Sr_{0.5}CoO_{3-\delta}$-SDC and LSCF-GDC.[44,45] It should be noted that the present result is obtained with single phase $La_{0.4}Bi_{0.4}Sr_{0.2}FeO_{3-\delta}$ cathode. The cathode performance could be further improved by adding an electrolyte material to form a composite electrode.[41,43]

CONCLUSIONS

Bismuth is doped to $La_{0.8}Sr_{0.2}FeO_{3-\delta}$ to form a series of perovskites, $La_{0.8-x}Bi_xSr_{0.2}FeO_{3-\delta}$ ($0 \le x \le 0.8$). Their properties are evaluated as a function of Bi doping content. The crystal structure changes from orthorhombic structure to cubic structure when $x = 0.3$, and the lattice volume and oxygen vacancy concentration increase with x. The electrical conductivity decreases with x, while the activation energy (E_a) for conductivity increases, indicating increased oxygen ionic conduction at higher Bi dopant content. The oxygen chemical diffusion coefficient (D_{chem}) and chemical surface exchange coefficient (K_{chem}) are evaluated by ECR measurement, and both D_{chem} and K_{chem} increase with bismuth content. Analysis of electrochemical impedance spectra shows enhanced catalytic activity for oxygen reduction reaction with Bi doping. Although the interfacial polarization resistance decreases with x, $La_{0.4}Bi_{0.4}Sr_{0.2}FeO_{3-\delta}$ is suggested as the most promising potential cathode material since it possesses small R_p and high electrical conductivity.

ASSOCIATED CONTENT

Supporting Information

The typical ECR experimental data and the fitting results for $La_{0.8-x}Bi_xSr_{0.2}FeO_{3-\delta}$ ($0 \le x \le 0.8$). This material is available free of charge via the Internet at http://pubs.acs.org.

AUTHOR INFORMATION

Corresponding Author

*Tel: ++86-551-63607475. Fax: ++86-551-63601696. E-mail: xiacr@ustc.edu.cn.

Funding

We gratefully acknowledge the financial support of the Ministry of Science and Technology of China (2012CB215403), the National Nature Science Foundation of China (51372239), and the U.S. National Science Foundation (DMR-1210792).

Notes

The authors declare no competing financial interest.

REFERENCES

(1) Ormerod, R. M. Solid Oxide Fuel Cells. *Chem. Soc. Rev.* **2003**, *32*, 17–28.

(2) Niu, Y.; Sunarso, J.; Zhou, W.; Liang, F.; Ge, L.; Zhu, Z.; Shao, Z. Evaluation and Optimization of $Bi_{1-x}Sr_xFeO_{3-\delta}$ Perovskites as Cathodes of Solid Oxide Fuel Cells. *Int. J. Hydrogen Energy* **2011**, *36*, 3179−3186.
(3) Simner, S. P.; Bonnett, J. R.; Canfield, N. L.; Meinhardt, K. D.; Shelton, J. P.; Sprenkle, V. L.; Stevenson, J. W. Development of Lanthanum Ferrite SOFC Cathodes. *J. Power Sources* **2003**, *113*, 1−10.
(4) Ralph, J. M.; Rossignol, C.; Kumar, R. Cathode Materials for Reduced-Temperature SOFCs. *J. Electrochem. Soc.* **2003**, *150*, A1518−A1522.
(5) Sun, S.; Zhu, X.; Yuan, Y. Electrochemical Properties of $La_{0.8}Sr_{0.2}FeO_{3-\delta}$ −$La_{0.45}Ce_{0.55}O_{2-\delta}$ Composite Cathodes for Intermediate Temperature SOFC. *J. Solid State Electrochem.* **2010**, *14*, 2257−2260.
(6) Myung, C. K.; Park, S. J.; Haneda, H. High Tempreture Electrical Conductivity of $La_{1-x}Sr_xFeO_{3-\delta}$ ($x > 0.5$). *Solid State Ionics* **1990**, *40/41*, 239−243.
(7) Mizusaki, J.; Sasamoto, T.; Cannon, W. R.; Bowen, H. K. Electronic Conductivity, Seebeck Coefficient, and Defect Structure of $La_{1-x}Sr_xFeO_3$ (x=0.1, 0.25). *J. Am. Ceram. Soc.* **1983**, *66*, 247−252.
(8) Bongio, E. V.; Black, H.; Raszewski, F. C.; Edwards, D. Microstructural and High-Temperature Electrical Characterization of $La_{1-x}Sr_xFeO_{3-\delta}$. *J. Electroceram.* **2005**, *14*, 193−198.
(9) Ren, Y.; Küngas, R.; Gorte, R. J.; Deng, C. The Effect of A-site Cation (Ln=La, Pr, Sm) on the Crystal Structure, Conductivity and Oxygen Reduction Properties of Sr-Doped Ferrite Perovskites. *Solid State Ionics* **2012**, *212*, 47−54.
(10) Tietz, F.; Arulraj, I.; Zahid, M.; Stover, D. Electrical Conductivity and Thermal Expansion of $La_{0.8}Sr_{0.2}(Mn,Fe,Co)O_{3-\delta}$ Perovskites. *Solid State Ionics* **2006**, *177*, 1753−1756.
(11) Wang, W.; Huang, Y.; Jung, S.; Vohs, J. M.; Gorte, R. J. A Comparison of LSM, LSF, and LSCo for Solid Oxide Electrolyzer Anodes. *J. Electrochem. Soc.* **2006**, *153*, A2066−A2070.
(12) Martínez-Amesti, A.; Larrañaga, A.; Rodríguez-Martínez, L. M.; Aguayo, A. T.; Pizarro, J. L.; Nó, M. L.; Laresgoiti, A.; Arriortua, M. I. Reactivity between $La(Sr)FeO_3$ Cathode, Doped CeO_2 Interlayer and Yttria-Stabilized Zirconia Electrolyte for Solid Oxide Fuel Cell Applications. *J. Power Sources* **2008**, *185*, 401−410.
(13) Wedig, A.; Lynch, M. E.; Merkle, R.; Maier, J.; Liu, M. Sheet Resistance in Thin Film Solid Oxide Fuel Cell Model Cathodes A Case Study on Circular $Bi_{1-x}Sr_xFeO_{3-\delta}$ Microelectrodes. *ECS Trans.* **2012**, *45*, 213−224.
(14) Niu, Y.; Sunarso, J.; Liang, F.; Zhou, W.; Zhu, Z.; Shao, Z. A Comparative Study of Oxygen Reduction Reaction on Bi- and La-Doped $SrFeO_{3-\delta}$ Perovskite Cathodes. *J. Electrochem. Soc.* **2011**, *158*, B132−B138.
(15) Wedig, A.; Merkle, R.; Stuhlhofer, B.; Habermeier, H. U.; Maier, J.; Heifets, E. Fast Oxygen Exchange Kinetics of Pore-Free $Bi_{1-x}Sr_xFeO_{3-\delta}$ Thin Films. *Phys. Chem. Chem. Phys.* **2011**, *13*, 16530−16533.
(16) Wang, L. Y.; Wang, D. H.; Huang, H. B.; Han, Z. D.; Cao, Q. Q.; Gu, B. X.; Du, Y. W. The Magnetic Properties of Polycrystalline $Bi_{1-x}Sr_xFeO_3$ Ceramics. *J. Alloys Compd.* **2009**, *469*, 1−3.
(17) Ding, D.; Liu, B.; Zhu, Z.; Zhou, S.; Xia, C. High Reactive $Ce_{0.8}Sm_{0.2}O_{1.9}$ Powders Via A Carbonate Co-precipitation Method As Electrolytes for Low-Temperature Solid Oxide Fuel Cells. *Solid State Ionics* **2008**, *179*, 896−899.
(18) Wang, Y.; Zhang, L.; Xia, C. R. Enhancing Oxygen Surface Exchange Coefficients of Strontium-Doped Lanthanum Manganates with Electrolytes. *Int. J. Hydrogen Energy* **2012**, *37*, 2182−2186.
(19) Wang, Y.; Wang, Y.; Xia, C. Surface Process of Doped Ceria Reduction by Electrical Conductivity Relaxation. *J. Electrochem. Soc.* **2012**, *159*, F570−F576.
(20) Bouwmeester, H. J. M.; Otter, M. W.; Boukamp, B. A. Oxygen Transport in $La_{0.6}Sr_{0.4}Co_{1-y}FeyO_{3-\delta}$. *J. Solid State Electrochem.* **2004**, *8*, 599−605.
(21) Yasuda, I.; Hishinuma, M. Electrical Conductivity and Chemical Diffusion Coefficient of Strontium-Doped Lanthanum Manganites. *J. Solid State Chem.* **1996**, *123*, 382−390.
(22) Zhao, F.; Zhang, L.; Jiang, Z. Y.; Xia, C. R.; Chen, F. L. A High Performance Intermediate-Temperature Solid Oxide Fuel Cell Using Impregnated $La_{0.6}Sr_{0.4}CoO_{3-\delta}$ Cathode. *J. Alloys Compd.* **2009**, *487*, 781−785.
(23) Larson, A. C.; Von Dreele, R. B. General Structure Analysis System (GSAS). *Los Alamos Natl. Lab. Rep. LAUR* **1994**, 86−748.
(24) Laarif, A.; Theobald, F. The Lone Pair Concept and the Conductivity of Bismuth Oxides Bi_2O_3. *Solid State Ionics* **1986**, *21*, 183−193.
(25) Dadyburjor, D. B.; Ruckenstein, E. Activation-Energies to Characterize Ease of Removal of Various Kinds of Oxygen from Bismuth Molybdate. *J. Catal.* **1980**, *63*, 383−388.
(26) Tai, L. W.; Nasrallah, M. M.; Anderson, H. U.; Sparlin, D. M.; Sehlin, S. R. Structure and Electrical-Properties of $La_{1-x}Sr_xCo_{1-y}Fe_yO_3$.1. The System $La_{0.8}Sr_{0.2}Co_{1-y}Fe_yO_3$. *Solid State Ionics* **1995**, *76*, 259−271.
(27) Ullmann, H.; Trofimenko, N.; Tietz, F.; Stover, D.; Ahmad-Khanlou, A. Correlation between Thermal Expansion and Oxide Ion Transport in Mixed Conducting Perovskite-Type Oxides for SOFC Cathodes. *Solid State Ionics* **2000**, *138*, 79−90.
(28) Tu, H.; Takeda, Y.; Imanishi, N.; Yamamoto, O. $Ln_{0.4}Sr_{0.6}Co_{0.8}Fe_{0.2}O_{3-\delta}$ (Ln= La, Pr, Nd, Sm, Gd) for the Electrode in Solid Oxide Fuel Cells. *Solid State Ionics* **1999**, *117*, 277−281.
(29) Khan, W.; Naqvi, A. H.; Gupta, M.; Husain, S.; Kumar, R. Small Polaron Hopping Conduction Mechanism in Fe Doped $LaMnO_3$. *J. Chem. Phys.* **2011**, *135*, 1−6.
(30) Stevenson, J. W.; Armstrong, T. R.; Carneim, R. D.; Pederson, L. R.; Weber, W. J. Electrochemical Properties of Mixed Conducting Perovskites $La_{1-x}M_xCo_{1-y}Fe_yO_{3-\delta}$ (M=Sr,Ba,Ca). *J. Electrochem. Soc.* **1996**, *143*, 2722−2729.
(31) Zener, C. Interaction between the d-Shells in the Transition Metals. II. Ferromagnetic Compounds of Manganese with Perovskite Structure. *Phys. Rev.* **1951**, *82*, 403−405.
(32) la O', G. J.; Shao-Horn, Y. Oxygen Surface Exchange Kinetics on Sr-Substituted Lanthanum Manganite and Ferrite Thin-Film Microelectrodes. *J. Electrochem. Soc.* **2009**, *156*, B816−B824.
(33) Zhang, L.; Liu, Y.; Zhang, Y.; Xiao, G.; Chen, F.; Xia, C. Enhancement in Surface Exchange Coefficient and Electrochemical Performance of $Sr_2Fe_{1.5}Mo_{0.5}O_6$ Electrodes by $Ce_{0.8}Sm_{0.2}O_{1.9}$ Nanoparticles. *Electrochem. Commun.* **2011**, *13*, 711−713.
(34) Lane, J. A.; Kilner, J. A. Measuring Oxygen Diffusion and Oxygen Surface Exchange by Conductivity Relaxation. *Solid State Ionics* **2000**, *136*, 997−1001.
(35) Lane, J. A.; Benson, S. J. Oxygen Transport in $La_{0.6}Sr_{0.4}Co_{0.2}Fe_{0.8}O_{3-\delta}$. *Solid State Ionics* **1999**, *121*, 201−208.
(36) ten Elshof, J. E.; Lankhorst, M. H. R.; Bouwmeester, H. J.M. Oxygen Exchange and Diffusion Coefficients of Strontium-Doped Lanthanum Ferrites by Electrical Conductivity Relaxation. *J. Electrochem. Soc.* **1997**, *144*, 1060−1067.
(37) Gao, J. F.; Lang, Y.; Xia, C.; Meng, G. Preparation and Electrochemical Properties of $La_{0.7}Sr_{0.3}FeO_{3-\delta}$ - $Sm_{0.2}Ce_{0.8}O_3$ Composite Cathodes. *Chin. J. Mater. Res.* **2005**, *19*, 72−77.
(38) Adler, S.; Chen, X.; Wilson, J. Mechanisms and Rate Laws for Oxygen Exchange on Mixed-Conducting Oxide Surfaces. *J. Catal.* **2007**, *245*, 91−109.
(39) Escudero, M. J.; Aguadero, A.; Alonso, J. A.; Daza, L. A Kinetic Study of Oxygen Reduction Reaction on La_2NiO_4 Cathodes by Means of Impedance Spectroscopy. *J. Electroanal. Chem.* **2007**, *611*, 107−116.
(40) Ralph, J. M.; Schoeler, A. C.; Krumpelt, M. Materials for Lower Temperature Solid Oxide Fuel Cells. *J. Mater. Sci.* **2001**, *36*, 1161−1172.
(41) Xia, C. R.; Rauch, W.; Chen, F. L.; Liu, M. L. $Sm_{0.5}Sr_{0.5}CoO_3$ Cathodes for Low-Temperature SOFCs. *Solid State Ionics* **2002**, *149*, 11−19.
(42) Liu, M. L.; Hu, H. X. Effect of Interfacial Resistance on Determination of Transport Properties of Mixed-Conducting Electrolytes. *J. Electrochem. Soc.* **1996**, *143*, L109−L112.
(43) Jiang, S. P. Activation, Microstructure, and Polarization of Solid Oxide Fuel Cell Cathodes. *J. Solid State Electrochem.* **2007**, *11*, 93−102.

(44) Xia, C. R.; Chen, F. L.; Liu, M. L. Reduced-Temperature Solid Oxide Fuel Cells Fabricated by Screen Printing. *Electrochem. Solid-State Lett.* **2001**, *4*, A52−A54.
(45) Leng, Y. J.; Chan, S. H.; Jiang, S. P.; Khor, K. A. Low-Temperature SOFC with Thin Film GDC Electrolyte Prepared in Situ by Solid-State Reaction. *Solid State Ionics* **2004**, *170*, 9−15.